Nuclear Instruments and Methods in Physics Research A 1063 (2024) 169262

Contents lists available at ScienceDirect

Nuclear Inst. and Methods in Physics Research, A

journal homepage: www.elsevier.com/locate/nima

Depletion depth studies with the MALTA2 sensor, a depleted monolithic active pixel sensor

D.V. Berlea [a,b,*], P. Allport [c], I. Asensi Tortajada [d], P. Behera [e], D. Bortoletto [f], C. Buttar [g], F. Dachs [d], V. Dao [d], G. Dash [e], D. Dobrijevic [d,h], L. Fasselt [a,b], L. Flores Sanz de Acedo [d], M. Gazi [f], L. Gonella [c], V. Gonzalez [i], G. Gustavino [d], P. Jana [e], M. LeBlanc [d], L. Li [c], H. Pernegger [d], P. Riedler [d], W. Snoeys [d], C.A Solans Sanchez [d], T. Suligoj [h], M. van Rijnbach [d], M. Vázquez Nuñez [d], A. Vijay [e], J. Weick [d,j], S. Worm [a,b], A.M. Zoubir [j]

[a] Deutsches Elektronen-Synchrotron DESY, Platanenallee 6, 15738, Zeuthen, Germany
[b] Institut für Physik, Humboldt-Universität zu Berlin, Newtonstrasse 15, 12489, Berlin, Germany
[c] University of Birmingham, Edgbaston Park Rd, B15 2TT, Birmingham, United Kingdom
[d] CERN, Esplanade des Particules 1, 1211, Meyrin, Switzerland
[e] Indian Institute of Technology Madras, Hostel Ave, Tamil Nadu 600036, Chennai, India
[f] University of Oxford, Keble Road, OX1 3RH, Oxford, United Kingdom
[g] University of Glasgow, University Ave, G12 8QQ, Glasgow, United Kingdom
[h] University of Zagreb, Ul. Radoslava Cimermana 88, 10000, Zagreb, Croatia
[i] Universitat de València, Avinguda Blasco Ibáñez, 13, 46010, Valencia, Spain
[j] TU Darmstadt, Karolinenplatz 5 64289, Darmstadt, Germany

ARTICLE INFO

Keywords:
MALTA
DMAPS
Silicon pixel
Detector
Monolithic
Depletion depth

ABSTRACT

MALTA2 is a depleted monolithic active pixel sensor (DMAPS) developed in the Tower 180 nm CMOS imaging process. Monolithic CMOS sensors offer advantages over current hybrid imaging sensors both in terms of increased tracking performance due to lower material budget but also in terms of ease of integration and construction costs due to the monolithic design. Current research and development efforts are aimed towards radiation-hard designs up to 100 Mrad in Total Ionizing Dose and 3×10^{15} 1 MeV n_{eq}/cm^2 in Non-Ionizing Energy Loss. One important property of a sensor's radiation hardness is the depletion depth at which efficient charge collection is achieved via drift movement. Grazing angle test-beam data was taken during the 2023 SPS CERN test beam with the MALTA telescope and Edge Transient Current Technique studies were performed at DESY in order to develop a quantitative study of the depletion depth for un-irradiated, epitaxial MALTA2 samples. The study is planned to be extended for irradiated and Czochralski MALTA2 samples.

1. The MALTA2 sensor

The MALTA sensor is a Depleted Monolithic Active Pixel Sensor (DMAPS) featuring a small collection electrode, fabricated in the Tower 180 nm feature size process. The monolithic design offers multiple advantages for tracking applications such as small radiation lengths (100–300 μm sensor thickness), low power dissipation (~1 μW/pixel) and high granularity (36.4 × 36.4 μm^2 pixel pitch). Additionally, the small collection electrode design leads to a low sensor capacitance (<5 fF) and to a larger signal amplitude and signal to noise ratio for relatively thin devices [1].

MALTA2 is the second generation of the MALTA sensor family. It has a 512 × 224 pixel array and brings improvements over the original sensor design [2]. The new design implements a cascode readout stage and enlarged transistors in the front-end amplifiers that in turn lowers the Random Telegraph Signal (RTS) noise component and shifts the operating threshold to lower values (~100 e^-) [3]. Additionally, a more efficient sensor configuration was realized by incorporating a shift register-based slow control [4].

Fig. 1 shows the MALTA pixel cross-section [5]. A low doped n-type implant (L-dop) is used to extend the depletion laterally across the entire pixel. Additionally, two modifications to the standard process have been added: a gap in the n-layer (NGAP) and an extra deep p-well implant (XDPW) [6]. They both are designed to shape the electric field in the pixel corners, such that the charge carriers avoid the electric

* Corresponding author at: Deutsches Elektronen-Synchrotron DESY, Platanenallee 6, 15738, Zeuthen, Germany.
E-mail address: vlad.berlea@desy.de (D.V. Berlea).

https://doi.org/10.1016/j.nima.2024.169262
Received 14 February 2024; Received in revised form 29 February 2024; Accepted 16 March 2024
Available online 19 March 2024

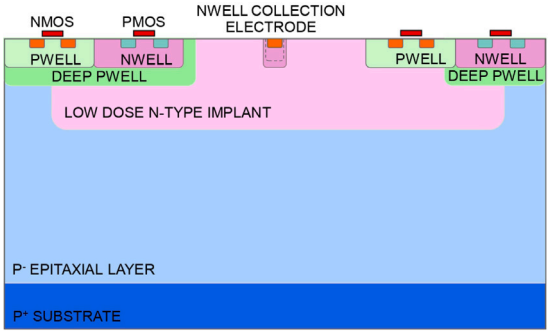

(a) NGAP processing.

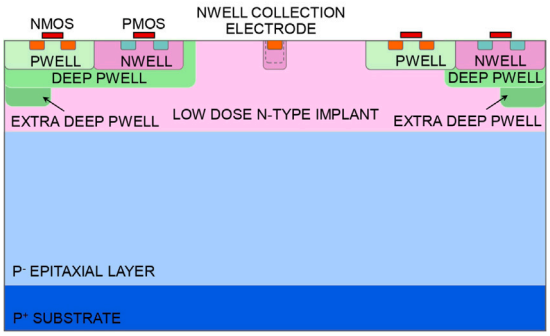

(b) XDPW processing.

Fig. 1. Cross section of the modified process, implementing a small electrode pixel. The n-layer extends the junction to the full pixel size. Two variations of this process are presented: modified process where the low dose n-implant is removed at the edge of the pixel (NGAP) (a) and an extra deep p-well is added at the edge of the pixel (XDPW) (b).

field minima points at the pixel corners (due to the double junction field potential) [7]. Both modifications were found to have a similar effect in terms of efficiency and radiation hardness.

Several test beam campaigns have been performed at the CERN Super Proton Synchrotron (SPS) facility, between 2021 and 2023 in order to characterize the novel MALTA2 sensor. The MALTA-based beam telescope [8] is a permanent installation in the North Area beam line and was used for triggering and characterization of the efficiency and timing measurements. The MALTA2 sensor was characterized in terms of hit efficiency, cluster size and timing performance [9] before and after neutron [10] and X-ray irradiation [3].

A decrease in depletion propagation leads to a degradation of all tracking figures of merit, making it an important sensor parameter to be studied. Measurements of the depletion depth within the pixel aim to shed light on the sensor performance at various pixel comparator thresholds and bias values. A systematic study of the depletion also aims to characterize the impact of process modifications on the electric field propagation. A detailed understanding of the hit collection efficiency allows for a sensor configuration optimization in future applications.

This study uses two methods for measuring the depletion depth of the MALTA2 sensors: a direct investigation of the depletion depth with a pulsed laser set-up (Edge Transient Current Technique [11]) and an indirect investigation method (the grazing angle technique [12]) performed with the MALTA telescope at SPS. An un-irradiated epitaxial silicon sample was used in this study. The low resistivity epitaxial layer has a 30 μm thickness, with a total sensor thickness of 100 μm and 300 μm respectively for mechanical support.

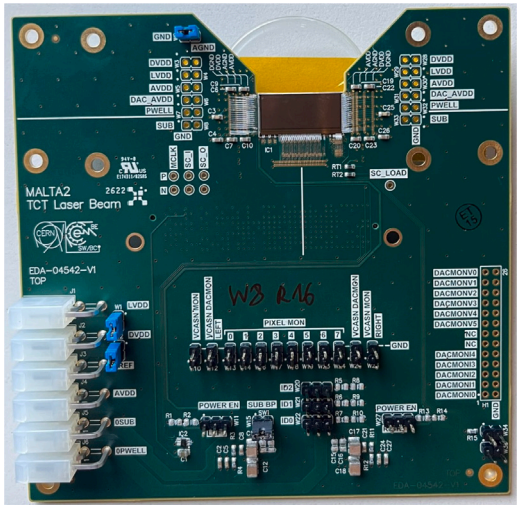

Fig. 2. MALTA2 carrier board layout for E-TCT with a wide opening at the top.

2. The Edge Transient Current Technique

The Edge Transient Current Technique (E-TCT) [11] uses a highly focused pulsed laser incident on the edge of the sensor. This technique acts as a very precise charge injection that aims to characterize a sensor's charge collection efficiency at various well-defined positions inside the silicon bulk. By scanning the laser across a pixel edge, a 2D map of the charge collection of a pixel can be made.

In order to access the edge of the MALTA2 sensor, the standard carrier board was redesigned to allow the laser to penetrate the sensor. Fig. 2 shows the new design of the PCB for E-TCT study. In order to minimize any laser non-uniformities, before wire bonding, the sensors were edge polished. The edge polishing was performed by manually applying a fine diamond paste (0.1 μm granularity) and repeatedly stroking with a cotton bud. For mechanical support and in order to avoid any static discharge on the sensor during polishing, the sensor was fixed with Kapton tape between two plastic blocks. Ref. [13] gives an in-depth explanation of best practices for edge polishing of a thin sensor. Finally, the sensor surface was cleaned with de-ionized water and prepared for wire bonding. Fig. 3 shows the MALTA sensor edge before (a) and after (b) polishing. After stealth dicing (laser ablation, followed by a tape expansion process [14]), several irregularities can be observed on the sensor edge. They are polished away and a smooth surface is achieved.

A pulsed Infra Red laser (1064 nm wavelength, 500 Hz frequency) was used for the E-TCT measurements of the MALTA2 sensor. Fig. 4 shows the E-TCT experimental set-up. The scanning of the sensor is performed by illuminating the pixel edge with the laser head and moving the linear stage in two axes (pitch and depth). Fig. 5 shows an expanded view of a pixel cross-section and highlights the two axes of movement of the stage: the pitch (across the sensor length) and depth (in the silicon bulk depth) axes. Additionally, the laser head can be moved on the height axis (down the matrix of the sensor).

Special analog pixels that bypass the normal digital operation of the pixel array are present at the matrix edges. The signal from these pixels can be read with a differential probe via an oscilloscope. Each measurement point of a detected amplitude is achieved by averaging 200 consecutive pulses.

2.1. Focus scan

To determine the minimum spot size and the focus position of the laser, a focus scan was performed. To measure the width of the beam, the laser is shone across the edge of the sensor in the depth axis.

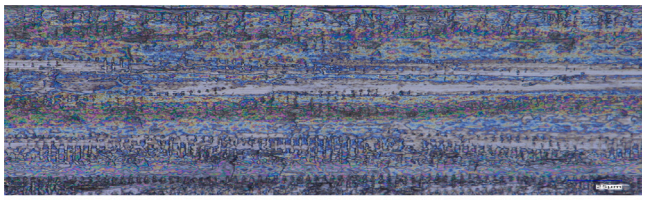

(a) Before Polishing.

(b) After Polishing.

Fig. 3. MALTA2 sensor edge before polishing (a) and after polishing (b).

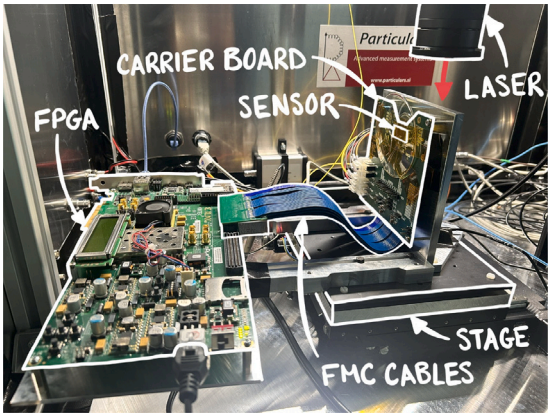

Fig. 4. E-TCT experimental setup. It consists of a sensor wire bonded to a specially designed PCB with a cut-out which allows laser penetration. The sensor slow control is performed with an FPGA and the analog readout is performed with a probe to an oscilloscope.

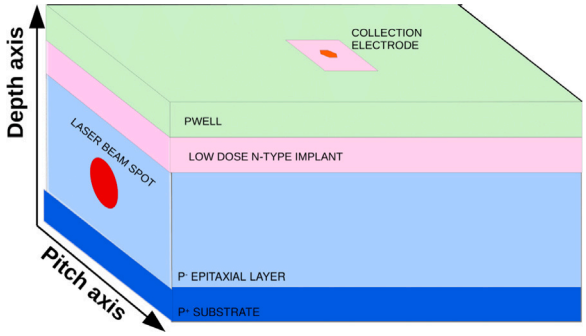

Fig. 5. Expanded view of a MALTA pixel cross-section. The orientation of the pitch and depth axes are marked and the laser spot position on the sensor edge is highlighted.

As the laser is scanned across the pixel, the signal turn-on near the pixel collection electrode gives a quantitative measurement of the beam width via the error function [13]:

$$f(x, A, \mu, \delta) = A\left(\mathrm{erf}\left(\frac{x-\mu}{\delta}\right) + 1\right),$$

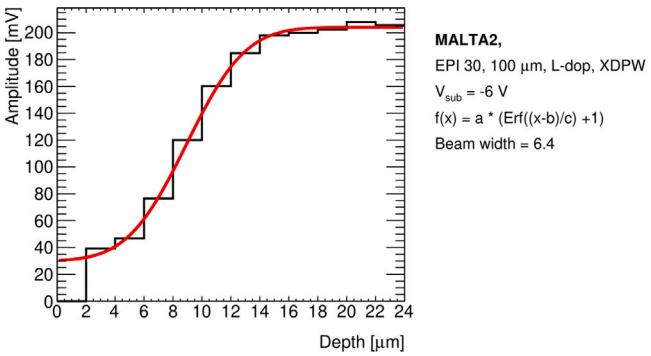

Fig. 6. Average amplitude recorded for multiple measured signals induced with the E-TCT laser at different depths in the pixel near the collection electrode for a fixed height. The data is fitted with an error function.

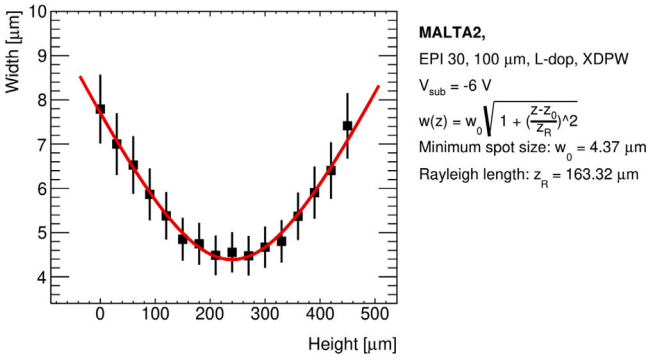

Fig. 7. The focus scan performed for a MALTA2 sample. The width calculated through the error function fit of multiple focus configurations is plotted versus the height position of the laser head. The data is fitted with a waist function for a Gaussian beam from which the best focus position and smallest beam width are extracted.

$$\mathrm{erf}\left(\frac{x-\mu}{\delta}\right) = \frac{2}{\sqrt{\pi}} \int_0^{\frac{x-\mu}{\delta}} e^{-\tau^2} d\tau$$

The fitting parameter A is proportional to the maximum of the charge profile and μ to the position of the edge corner. The beam width is deduced from the width parameter of the error function, δ as $\omega = \sqrt{2}\delta$ [13]. Fig. 6 shows a depth scan near the collection electrode for a laser focus configuration. The focus scan consists of measuring multiple laser widths at different laser heights, shown in Fig. 7. The data is fitted with a waist function for a Gaussian beam:

$$w(z) = w_0 \sqrt{1 + \left(\frac{z - z_0}{z_R}\right)^2}$$

The minimum spot size is found to be 4.4 ± 0.4 µm and the Rayleight length, $z_R = 163 \pm 16$ µm.

2.2. E-TCT results

A 2D scan of the analog pixel edge has been performed for multiple bias values: −6 V, −8 V and −10 V. Fig. 8 shows the evolution of the depth and pitch depletion with the increase in bias voltage. The overlaid red box estimates the position of the pixel projection in the 2 axes (36.4 µm pitch dimension and 30 ± 2 µm depth maximum size). The maximum charge collection efficiency follows a distribution which shows a larger electric field near the collection electrode laterally (pitch) and horizontally (depth). This effect was simulated with TCAD [7] and is attributed to the lightly doped n-layer which provides an enhanced lateral electric field. The extra deep p-well modification suppresses the electric field near the pixel corners which limits the lateral depletion along the pitch axis [15].

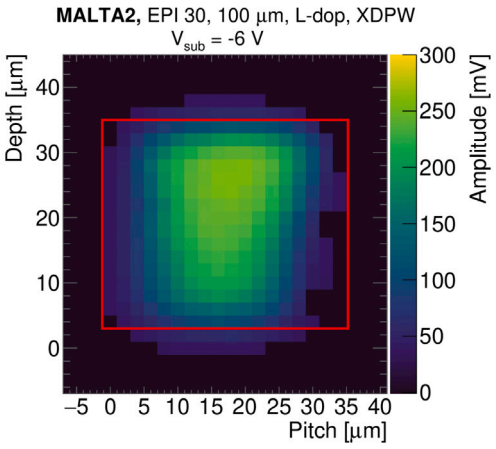

(a) −6V bias.

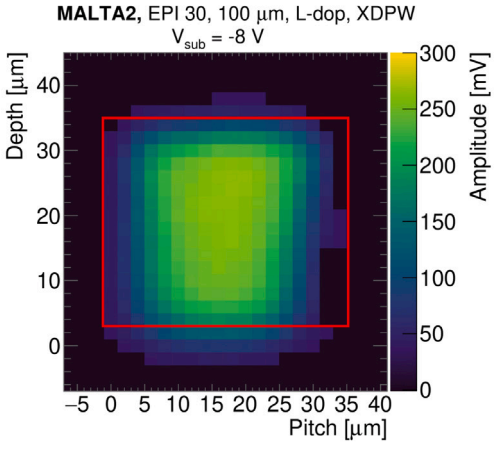

(b) −8V bias.

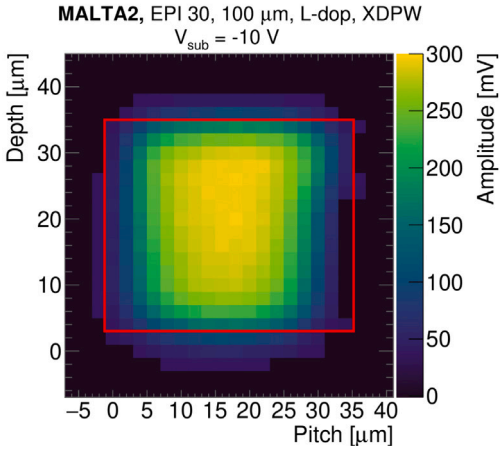

(c) −10V bias.

Fig. 8. 2D distribution of analog signal amplitudes induced with an E-TCT for multiple bias values of the sensor: −6 V (a), −8 V (b) and −10 V (c). The orientation of the plot is such that the collection electrode sits at the top of the plot and the sensor edge on the left.

Fig. 9 shows the projection of Fig. 8 in the pitch direction. The top plot shows the data normalized to the maximum value of the −10 V bias measurement point and the bottom plot shows the data normalized to each distribution maximum. Both normalizations highlight a symmetric distribution around the pixel collection electrode. This is expected due to the octagonal electrode and symmetrical pixel pitch design [7]. The lateral depletion is calculated as the Full Width at Half Maximum (FWHM) of the projection distribution. The estimation of the depletion is additionally convoluted with the Gaussian smearing of a ∼4 µm wide beam. The lower amplitudes at smaller bias values are compatible with fewer collected charges. As expected, a larger bias voltage leads to larger collected amplitudes. A systematic increase of the lateral depletion is observed with an increase in the bias voltage, from 23.6 µm at −6 V, to 25 µm at −10 V. The lateral depletion can be improved by further optimization of the electrical field design, in order to achieve the full 36.4 µm lateral dimension.

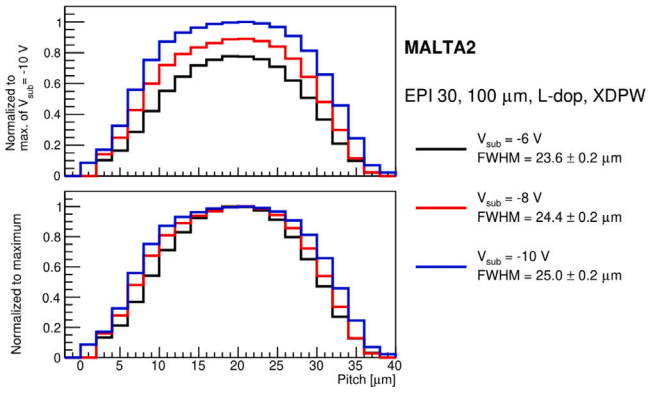

Fig. 9. Projection on the pitch axis of the measured amplitude distribution with the E-TCT for multiple bias voltages: −6, −8, −10 V. Two normalization procedures are performed on the data. A normalization to the maximum value of the −10 V SUB bias amplitude distribution is performed in the top plot and a normalization to the respective maximum amplitude of the distributions in the bottom plot.

Fig. 10 shows the projection of Fig. 8 in the depth direction. Unlike the pitch projection, it shows an asymmetrical distribution. It is characterized by a rapid increase near the collection electrode, followed by a plateau and a slower decrease further in the silicon bulk. The normalization of the upper figure shows the increase in measured amplitude with bias voltage, due to the increase of the electric field strength. The bottom normalization highlights that at larger bias voltages, the depth distribution has a "flatter" plateau after the sharp increase near the collection electrode (depth ∼ 30 µm). This is an indication of a more uniform electric field in depth at higher bias voltages. The depletion depth estimation remains relatively unchanged for the various bias voltages, suggesting that the epitaxial layer is fully depleted in depth at −6 V and only an increase in the electric field strength is achieved by increasing the bias voltage.

3. The grazing angle technique

An additional, indirect investigation method of the depletion depth was performed. The grazing angle technique [12] uses a geometrical model that correlates the depletion depth of a sensor to the increase of the average cluster size due to the inclination of incident charged-particle (mixed hadron beam from the SPS facility) tracks:

$$Cl_{size\perp}(\tan\alpha) = \frac{d}{p}\tan\alpha + Cl_{size\perp}(0)$$

The average cluster size is defined as the average numbers of pixels above the comparator threshold associated to a single particle hit. $Cl_{size\perp}$ is the cluster size projected on the axis perpendicular to the axis of rotation, d is the active depth, p is the pixel pitch and α is the track angle. The active depth of a sensor configuration can be calculated from the slope of the increase in cluster size with track angle. A smearing of the estimated depth is expected at the boundary of the junction,

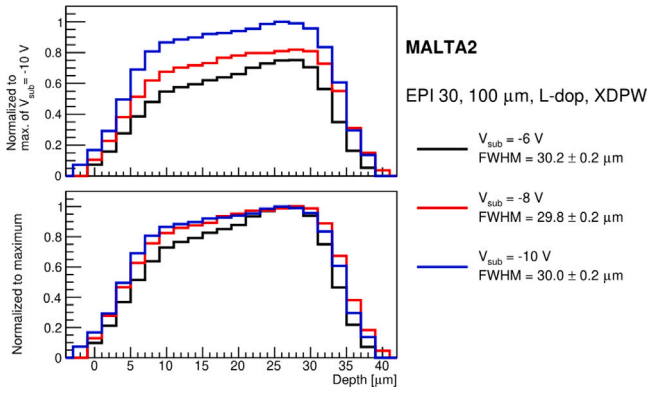

Fig. 10. Projection on the depth axis of the measured amplitude distribution with the E-TCT for multiple bias voltages: −6, −8, −10 V. Two normalization procedures are performed on the data. A normalization to the maximum value of the −10 V SUB bias amplitude distribution is performed in the top plot and a normalization to the respective maximum amplitude of the distributions in the bottom plot.

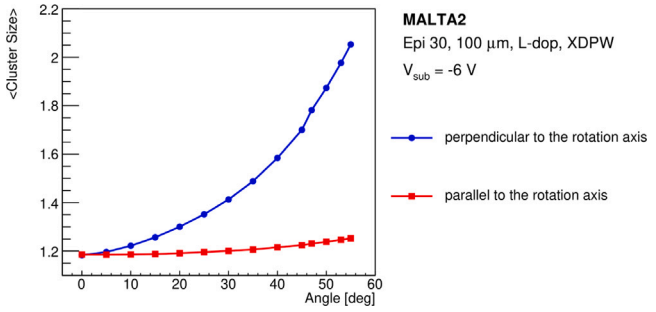

Fig. 11. Average cluster size projected on the perpendicular and parallel axis of rotation vs the angle of rotation for a MALTA2 sample.

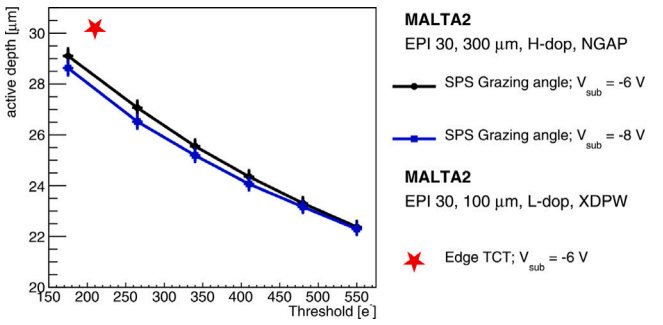

Fig. 12. Active depth versus threshold in electrons for two measurement techniques: grazing angle, performed with a 180 GeV hadron beam at SPS CERN and E-TCT, performed with a pulsed laser.

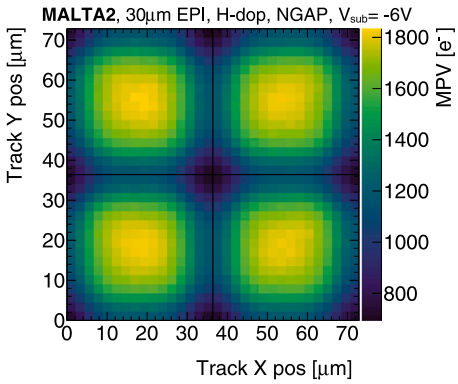

Fig. 13. Most probable value of the energy loss (MPV) projected onto a 2 × 2 pixel matrix. The MPVs are sorted into 2.3×2.3 µm^2 bins based on their associated track position within the pixel extracted from the telescope data. It is obtained by scanning the threshold in fine steps and fitting a cumulative Landau distribution to the efficiency spectrum.

where an electric field gradient is present. As a consequence, the active depth estimation approaches the depletion depth of the sensor, when the diffusion component of the collected charge is minimized. In order to generate inclined tracks through the sensor, the DUT was placed on a rotating stage that allowed the systematic rotation of the sensor.

While at low angles, the diffusion component of cluster formation is dominant, at large angles the cluster formation due to angled particle tracks is dominant. Fig. 11 shows the projections in the perpendicular (blue line and circles) and parallel (red line and squares) directions relative to the axis of rotation of the average cluster size for multiple angle values. The parallel projection remains constant with the increase in angled tracks. At larger angles, a slight increase in cluster size is noticed. It is correlated to both a tilt in the DUT plane and a larger total deposited energy of hits that lead to an increase in charge sharing. The perpendicular projection increases with the rotation angle. The increase is characterized by a diffusion dominated regime (angles < 30) and a linear regime for larger angles (angles > 30).

A systematic study of the active depth of an epitaxial MALTA2 sample has been performed for multiple pixel comparator threshold and bias voltage configurations as is shown in Fig. 12. Similar to the E-TCT results, the increase in bias over −6 V for an epitaxial sample does not lead to an increase in active depth, indicating a full depletion of the 30 µm thick substrate. The systematically lower measured active depth at higher bias is due to the increase in sensor noise at larger bias values, as seen in Ref. [10].

Fig. 13 shows the Most Probable Value (MPV) of the energy loss projected onto a 2 × 2 pixel matrix. A ∼50% drop between the charge collected in the pixel center and the pixel corner is observed. This is explained by the lower active depth at larger applied thresholds due to pixel boundary charge sharing.

Due to a limited diffusion component from the low resistivity silicon carrier wafer, the active depth estimation approaches the depletion depth for the lowest threshold value. This is additionally highlighted by comparing the E-TCT measurement point (red data point in Fig. 12) with the grazing angle technique measurements. The threshold for the E-TCT measurement point is deduced as the oscilloscope trigger value (∼30 mV) scaled to the MPV of a Minimum Ionizing Particle (MIP) passing through the sensor.

4. Conclusions

The active depth of the MALTA2 sensor has been measured by employing two methods: the E-TCT and the grazing angle technique. The E-TCT offers a direct measurement of the two-dimensional collected charge profile, but requires multiple preparatory steps: PCB redesign, edge polishing and analog read-out. The grazing angle technique has a straightforward implementation in an already existing beamline experiment, but has resolution only in the depth axis.

The two techniques show similar results for the lowest threshold configuration of the sensor measured with the grazing angle technique. The 30 µm epitaxial thick silicon is fully depleted in depth at −6 V bias, but an increase in the lateral depletion is observed at larger bias voltages, up to −10 V. Additionally, a more uniform electric field is highlighted at higher bias voltages.

The performed study shows important results in terms of pixel performance and future sensor configuration tuning for radiation hardness and efficient charge collection shape optimization. The measured epitaxial samples offered an important proof of concept for the two techniques and highlights the importance of both techniques in a

thorough depletion depth study. Further studies are planned, in order to measure the depletion depth of Czochralski silicon samples and irradiated samples that will offer further estimation of the radiation damage impact on the MALTA2 sensor.

Declaration of competing interest

The authors declare that they have no known competing financial interests or personal relationships that could have appeared to influence the work reported in this paper.

Acknowledgments

This project has received funding from the European Union's Horizon 2020 Research and Innovation programme under Grant Agreement numbers 101004761 (AIDAinnova), 675587 (STREAM), and 654168 (IJS, Ljubljana, Slovenia). We thank Alexandra Savino for the graphics and the photo shown in Fig. 4.

References

[1] W. Snoeys, Development of monolithic sensors for high energy physics in commercial CMOS technologies, Nucl. Instrum. Methods A 938 (2019) 41–50.
[2] F. Piro, et al., A 1-μW radiation-hard front-end in a 0.18-μm CMOS process for the MALTA2 monolithic sensor, IEEE Trans. Nucl. Sci. 69 (6) (2022) 1299–1309.
[3] D.V. Berlea, et al., Radiation hardness of MALTA2, a monolithic active pixel sensor for tracking applications, IEEE Trans. Nucl. Sci. 70 (10) (2023) 2303–2309.
[4] L. Flores Sanz de Acedo, et al., Latest developments and characterisation results of DMAPS in TowerJazz 180 nm for high luminosity LHC, in: J. Phys. Conf. Ser., Vol. 2374, 2022, 012169.
[5] H. Pernegger, et al., MALTA-cz: A radiation hard full-size monolithic CMOS sensor with small electrodes on high-resistivity Czochralski substrate, 2023, arXiv preprint: arXiv:2301.03912.
[6] M. Dyndal, et al., Mini-MALTA: Radiation hard pixel designs for small-electrode monolithic CMOS sensors for the high luminosity LHC, J. Instrum. 15 (02) (2020) P02005.
[7] M. Munker, et al., Simulations of CMOS pixel sensors with a small collection electrode, improved for a faster charge collection and increased radiation tolerance, J. Instrum. 14 (05) (2019) C05013.
[8] M. van Rijnbach, et al., Performance of the MALTA telescope, Eur. Phys. J. C 83 (7) (2023) 581.
[9] G. Gustavino, et al., Timing performance of radiation hard MALTA monolithic pixel sensors, J. Instrum. 18 (03) (2023) C03011.
[10] M. van Rijnbach, et al., Radiation hardness of MALTA2 monolithic CMOS sensors on Czochralski substrates, 2023, arXiv preprint: arXiv:2308.13231.
[11] R. Klanner, et al., Determination of the electric field in highly-irradiated silicon sensors using edge-TCT measurements, Nucl. Instrum. Methods A 951 (2020) 162987.
[12] S. Meroli, et al., A grazing angle technique to measure the charge collection efficiency for CMOS active pixel sensors, Nucl. Instrum. Methods A 650 (1) (2011) 230–234.
[13] F. Feindt, Edge-TCT for the Investigation of Radiation Damaged Silicon Strip Sensors (Ms), Universität Hamburg, Hamburg, 2017, p. 95, URL https://api.semanticscholar.org/CorpusID:55952401.
[14] P. Riedler, et al., Studies for low mass, large area monolithic silicon pixel detector modules using the MALTA CMOS pixel chip, Nucl. Instrum. Methods A 990 (2021) 164895.
[15] K. Dort, Simulation Studies and Characterisation of Monolithic Silicon Pixel-Detector Prototypes for Future Collider Detectors & Unsupervised Anomaly Detection in Belle II Pixel-Detector Data (PhD), University of Giessen, Germany, 2022, URL https://cds.cern.ch/record/2813457.